Electrochemistry

DOI: 10.1002/anie.201201488

Self-Assembled Germanium/Carbon Nanostructures as High-Power Anode Material for the Lithium-Ion Battery**

Kuok Hau Seng, Mi-Hee Park, Zai Ping Guo, Hua Kun Liu, and Jaephil Cho**

The automobile industry is currently shifting towards hybrid and electric vehicles which are powered by electrochemical energy storage systems. However, these "greener" alternatives still suffer from low mileage when compared to a full tank of gasoline. Therefore, it is important to develop batteries that have a high energy density, high power density, and long cycle life. Lithium-ion batteries (LIBs) have been widely used in the consumer market for portable electronic devices since their introduction in the 1990s. This battery system is a more suitable candidate for hybrid/electric vehicles compared to nickel metal hydride, alkaline, and lead–acid batteries because of its higher volumetric and gravimetric energy density. However, there is still room for improvement in the case of the energy and power densities of LIBs. One strategy to increase the performance of LIBs is to find alternative anode materials that satisfy both requirements.

Germanium is an excellent candidate as anode material for LIBs when compared to other metallic anode materials that undergo lithium alloying reactions, such as tin[1] and silicon.[2] This is because of its high theoretical capacity (1600 mA h g^{-1}, 4.4 Li^+ ions per Ge atom), good lithium diffusivity (400 times faster than in silicon), and high electrical conductivity (104 times higher than silicon). Nevertheless, the price of germanium is the major drawback for the commercialization of this anode material. Furthermore, similar to silicon and tin, germanium suffers large volume changes during lithium alloying/de-alloying reactions. With prolonged cycling, the mechanical stress causes electrode pulverization from the current collector, and this leads to capacity fading. Various approaches have been reported to enhance the cycling stability of germanium. These include using morphologies that have better structural stability for accommodating volume changes (nanoparticles,[3] nanowires,[4] nanotubes,[5] and porous[6] and mesoporous[7] structures), germanium-based composites (tin-germanium,[8] germanium/carbon nanotubes[9]), germanium oxides,[10] and carbon coating of germanium. However, rate capabilities of germanium anodes that have been reported need more improvement to satisfy the requirements of electric vehicles with high energy consumption.

Herein, we report a facile synthesis method to produce germanium/carbon nanostructures by carbon coating and reduction of the oxide precursor. When the particle size of the germanium oxide precursor was varied, two different self-assembled germanium/carbon nanostructures could be obtained, namely, a cluster (C) nanostructure and a non-clustered (NC) structure. Hereafter, they are denoted as "C-Ge/C" and "NC-Ge/C". Both germanium/carbon nanostructures displayed good cycling stability at the 0.2 C rate (0.32 A g^{-1}) for over 50 cycles and at the 1 C rate (1.6 A g^{-1}) for over 120 cycles. Surprisingly, the C-Ge/C structure shows an exceptionally high rate capability up to the 40 C rate (64 A g^{-1}). The NC-Ge/C structure, however, showed very poor capacity retention at rates over 1 C. These two extremes demonstrate the advantages of the nanostructured cluster, which will be further discussed.

A brief summary of the synthesis procedure is shown in Scheme 1. The germanium oxide nanoparticle precursors were prepared by hydrolysis of $GeCl_4$ in either a water/ethanol mixture (< 100 nm) or a reverse micelle water/heptane system (around 700 nm). Acetylene gas was chosen

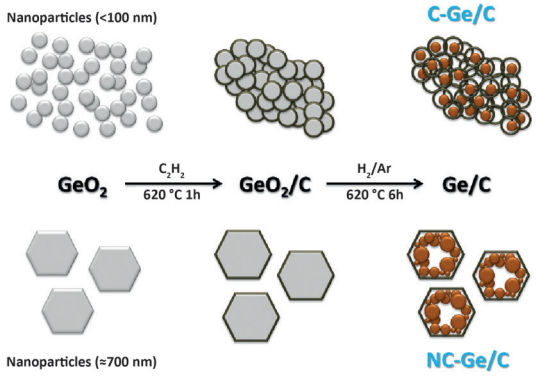

Scheme 1. Synthesis method to prepare self-assembled germanium/carbon nanostructures. Carbon coating on the precursors were achieved with acetylene/argon gas mixture at 620 °C. Then, germanium oxide was reduced by a hydrogen/argon gas mixture.

[*] K. H. Seng, Prof. Z. P. Guo, Prof. H. K. Liu
Institute for Superconducting and Electronic Materials
University of Wollongong, 2522 NSW (Australia)
E-mail: zguo@uow.edu.au
Homepage: http://isem.uow.edu.au
M. Park, Prof. J. Cho
Interdisciplinary School of Green Energy
Ulsan National Institute of Science and Technology (UNIST)
Ulsan, 689-798 (South Korea)
E-mail: jpcho@unist.ac.kr
Homepage: http://jpcho.com

[**] This work is supported by an Australian Research Council (ARC) discovery project (grant number DP1094261) and the ITRC (Information Technology Research Center) support program supervised by the NIPA (National IT Industry Promotion Agency) (grant number NIPA-2011-C1090-1100-0002). The authors would like to thank Dr. Tania Silver for critical reading of the manuscript and valuable remarks.

Supporting information for this article is available on the WWW under http://dx.doi.org/10.1002/anie.201201488.

as the carbon source because of its ability to form a uniform layer of carbon, and in the case of C-Ge/C, to simultaneously promote granulation of the composite, which is beneficial in reducing inhalation hazards associated with nanoparticles.[2e] Then, hydrogen gas was used as the reducing agent in a thermally induced reduction process at 620 °C to obtain metallic germanium. A similar approach has been reported recently by Yang and Venoit[11] using a GeO_2-like sol and anodic alumina oxide template to synthesize germanium nanowires.

Figure 1 shows transmission electron microscopy (TEM) images of the transformation from GeO_2 to Ge/C. After one hour of acetylene decomposition, a uniform carbon layer was deposited on the sample surface. The thickness of the carbon layer is around 3 to 5 nm and 6 to 10 nm, respectively, for the intermediates of the C-Ge/C and NC-Ge/C. A reaction time of 6 h is required (as shown in Figure S1a in the Supporting Information) to fully reduce GeO_2 to Ge, which agrees with what has been reported in the literature.[11] After completion of the reduction process, voids and pores appear inside the carbon shells in both samples because of the associated volume changes. In addition, the thickness of the carbon shell remained unchanged, signifying that the reduction process is mainly induced by hydrogen and not carbon. The C-Ge/C sample shows individual particles about 20 nm in size encapsulated in carbon shells, similar to a yolk/shell structure. Another important feature of this sample are the interconnected carbon shells (Figure 1 b and 1 c). Some empty shells are also seen in Figure 1 c, and this may be because of the aggregation with neighboring particles and further growth, as indicated by the denser areas. On the other hand, various particle sizes (20–200 nm) can be seen in the carbon shell of the NC-Ge/C. Most of the particles are aggregated near the inner surface of the carbon shell, forming a hollow core. To further determine the morphology and distribution of germanium in both samples, energy dispersive X-ray spectroscopy (EDS) analysis was performed. Figure S2 shows the element mapping of the corresponding micrograph of the C-Ge/C sample. Germanium was found to be mainly located inside the carbon shells. On the other hand, element mapping (see Figure S3 in the Supporting Information) and line scans (Figure S4) were performed on a disintegrated NC-Ge/C particle to give evidence of the hollow structure. Furthermore, the surface morphology of both samples was investigated using scanning electron microscopy (SEM). In Figure S5c and S5e, large clusters of up to 10 micrometers in size can be seen, indicating the successful granulation of the germanium nanoparticles, and this structure remained after the reduction process. As for the NC-Ge/C (Figure S6 in the Supporting Information), the sample is composed of mainly individual polyhedra about 700 nm in diameter with quasi-hexagonal shapes. After carbon coating and reduction, the size of the particles remained similar to that of the precursor, and no granulation was observed. Some disintegrated particles can be seen, and the hollow structure is also visible when inspected at higher magnification (Figure S6 f).

X-ray diffraction (XRD) was used to characterize the Ge/C samples and the precursors. The diffraction patterns (Figure S1) of the precursors and the Ge/C samples can be indexed to the hexagonal phase (ICDD# 36-1436) and the diamond cubic phase (ICDD# 04-0545), respectively. In addition, high-resolution transmission electron microscopy (HRTEM) was also performed on the Ge/C samples, and the micrographs are shown in Figure S7 in the Supporting Information. The lattice spacing was measured to be about 0.32 nm, matching the *d* spacing of (111) planes in cubic germanium. Fast Fourier transform (FFT) diffraction patterns, which are shown in the insets of the images, display patterns that correspond to the diamond cubic phase. Moreover, Raman spectroscopy was also performed on both Ge/C samples, as shown in Figure S8, and confirms the presence of crystalline germanium, which is represented by a sharp peak at 300 cm^{-1}. Two other peaks that are related to the D and G bands of carbon were also detected at 1337 and 1605 cm^{-1}. The intensity ratio of D/G for both samples was calculated (based on fitting a Gaussian function) to be 0.9, which represents microcrystalline graphitic carbon.[12] The level of surface oxidation of germanium particles was investigated using Fourier transform infrared (FTIR) spectroscopy (Figure S9). The NC-Ge/C shows a small hump at 882 cm^{-1} which is related to germanium oxide, but no germanium oxide peaks were detected in the C-Ge/C. However, EDS elemental mapping results show that only negligible amounts of oxygen are present in either of the samples (< 3 wt %). The carbon contents of the samples were investigated by

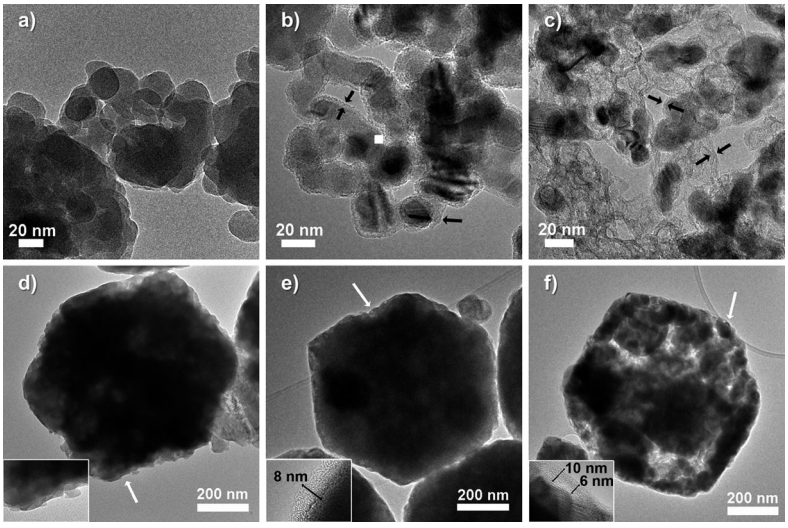

Figure 1. TEM images showing the formation of germanium/carbon nanostructures from the germanium oxide precursors. a) GeO_2 nanoparticles. b) Carbon-coated GeO_2 nanoparticles. c) C-Ge/C. The black arrows in (b,c) indicate that the carbon shells have a thickness of about 3 nm. d) Hexahedral-like GeO_2 (around 700 nm). e) Image of (d) after carbon coating. The inset shows the carbon layer at the area indicated by the white arrow. f) NC-Ge/C particle, which is made up of many germanium nanoparticles inside the carbon shell. The inset shows the carbon shell at the area indicated by the white arrow.

CHNS elemental analysis. They were determined to be 10 and 20 wt% in the NC-Ge/C and C-Ge/C structures, respectively. Figure S10 in the Supporting information shows the isotherm curves of both samples from Brunauer–Emmet–Teller (BET) analysis, and the insets are the pore size distributions calculated using the Barrett–Joyner–Halenda (BJH) desorption method. The total surface areas were determined to be 125 and 92 $m^2 g^{-1}$, respectively, for C-Ge/C and NC-Ge/C.

Figure 2a shows the cycling performance of both samples at the 0.2 C rate (0.32 $A g^{-1}$) for 50 cycles in the voltage range of 0.01 V to 1.5 V versus Li/Li^+. NC-Ge/C showed higher initial capacity compared to C-Ge/C because of the higher germanium content in the sample. The C-Ge/C sample showed excellent capacity retention with negligible capacity fading (95% retention) after 50 cycles, while 80% of capacity retention was recorded for NC-Ge/C. The inset of Figure 2a shows the first cycle voltage profiles of both samples. The first discharge and charge capacities (Q) were 1720 and 1184 mA h g^{-1}, respectively, for the C-Ge/C sample, corresponding to a coulombic efficiency of 70%. This is lower than for NC-Ge/C, for which a coulombic efficiency of 85% was recorded in the first cycle. The difference in efficiency is mainly due to the larger surface area of C-Ge/C, where more solid electrolyte interphase (SEI) layer is irreversibly formed. The electrochemical reaction of Ge/C was determined using differential plots (dQ/dV vs. V), as shown in Figure S11 in the Supporting Information, and the reaction mechanism is similar to that previously reported for other germanium anodes.[4c] Furthermore, capacity retention of both Ge/C samples at a 1 C rate was tested and the results are shown in Figure 2b. Capacity fading was observed until the 40th cycle, and then the capacity remained relatively stable for the subsequent cycles. The capacity retention recorded was 74% and 63%, respectively, for C-Ge/C (896 mA h g^{-1}) and NC-Ge/C (830 mA h g^{-1}) after 120 cycles. The specific capacity is still considerably higher (at the 1 C rate) when compared to previous reports in the literature,[3b,4,5,7–9,11,13] with the exception of a 3D porous Ge structure reported by us.[6] The higher capacity and cycling stability of the C-Ge/C and NC-Ge/C samples can be attributed to the hollow/porous carbon shells, which can accommodate the volume changes during lithium reactions. In addition, the porosity caused by the hollow carbon shells can also increase the electrolyte diffusion to the germanium nanoparticles. This is proven by the TEM images shown in Figure S12, where the general morphology of the sample after 120 cycles of charge/discharge remained similar to that of the freshly prepared sample for the C-Ge/C. Although the shape of the NC-Ge/C particles (Figure S12c) changed, no significant disintegration was observed, and the particle size is similar to that in the fresh sample. In both samples, amorphization of the germanium nanoparticles after long-term cycling was observed, which is similar to what occurs in other alloying anode materials.[14] Both samples were also tested for their rate performances, and the results

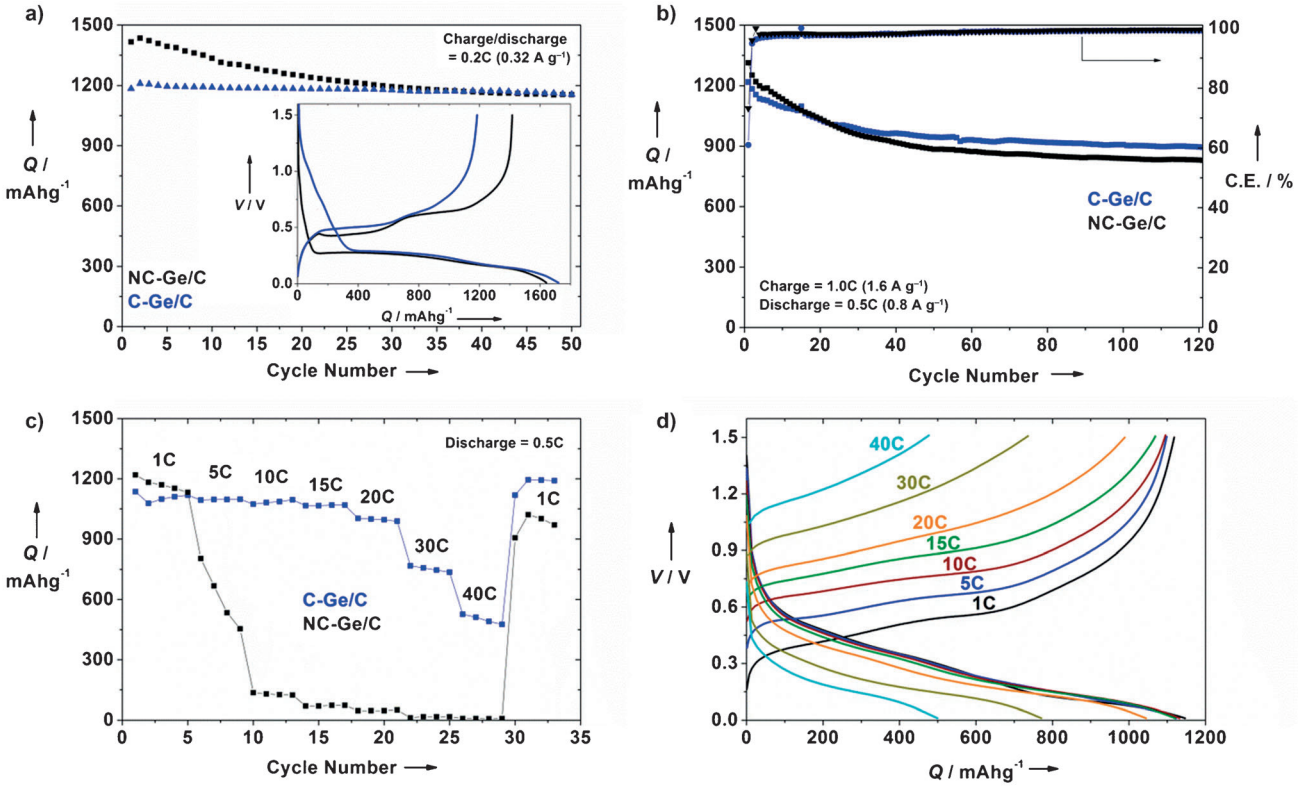

Figure 2. a) Cycling performance of the Ge/C samples at 0.2 C. The inset is the corresponding voltage profile of the first charge/discharge cycle. b) Cycling performance of the Ge/C samples at a 1 C charging rate over 120 cycles (C.E. = coulombic efficiency). c) Rate performance of the Ge/C samples with increasing rate from 1 to 40 C. d) Voltage profiles of C-Ge/C sample corresponding to the rate performance test in (c). All the cells were tested in the voltage range of 0.01–1.5 V versus Li/Li^+.

are plotted in Figure 2c. The NC-Ge/C sample showed poor capacity retention when the C-rate was increased to 5 C and above, but the capacity was recovered when the rate was returned to 1 C. The poor rate performance can be related to the polarization of the anode material at higher currents, which is evident in the voltage profiles shown in Figure S13. On the other hand, C-Ge/C showed excellent capacity retention at higher rates. Negligible capacity loss is recorded for up to 15 C, and the capacity retention at the 20 C rate is 91%. This is significantly higher than in our previously reported work on germanium nanotubes, which only managed to retain 60% capacity at 20 C.[5] When the rate was further increased to 40 C (64 $A g^{-1}$), the capacity retention was 44%, and the specific capacity recorded is exceptionally high at 480 $mAh g^{-1}$. The corresponding voltage profiles are plotted in Figure 2d. It should be noted that as the C rate is increased, the increase in polarization is much lower compared to the NC-Ge/C (Figure S13a). In addition, cycling performance at 20 and 40 C rates was also tested on the C-Ge/C sample. Figure S13b shows the cycling performance over 100 cycles. Gradual capacity fading at the initial cycles, similar to the 1 C test, was observed for both high-rate cycling tests. At 20 C, the capacity after 50 cycles is 600 $mAh g^{-1}$ and remained relatively stable when the sample is further cycled. For the test at 40 C, the capacity at the 50th cycle is 360 $mAh g^{-1}$ and remained stable for up to 100 cycles, which is comparable to the theoretical capacity of graphite (372 $mAh g^{-1}$). To the best of our knowledge, these are the highest capacity and rate capability ever reported for any anode material that undergoes a lithium alloying reaction.[1–9,11,13]

In summary, we have synthesized two Ge/C nanostructures through a facile self-assembly method. Controlling the size of the precursor germania nanoparticles produces a cluster and a non-clustered nanostructure. In both structures, the germanium nanoparticles were located inside the hollow carbon shells. The C-Ge/C showed better capacity retention and exceptionally high rate performance. Adding into consideration the facile synthetic method that forms the unique nanostructure by self-assembly, the C-Ge/C sample has the potential for being a high-energy and high-power anode material for lithium-ion batteries. We conclude that the superior electrochemical performance is due to the unique nanostructure, which provides good electrolyte diffusion in the pores and good electronic conductivity through the interconnected network of carbon shells. Nevertheless, the intrinsic properties of germanium, such as the Li diffusivity and electronic conductivity, also contributed to the electrochemical performance.

Experimental Section

The reduction and carbon coating processes were carried out in a horizontal tube furnace. The gases used in the experiment were 5% H_2 in argon, 10% C_2H_2 in argon, and 99.99% argon. In a typical experiment, an alumina boat containing GeO_2 was placed in the central heating zone of the tube furnace. The tube was evacuated to ultrahigh vacuum to eliminate air, and flowing argon gas was then introduced. The sample was then heated to 620 °C, argon was replaced by a acetylene gas/argon mixture, and the flow continued for 1 hour, and finally, this acetylene/argon mixture was replaced by a hydrogen/argon mixture, and the flow continued for 6 h. The furnace was then left to cool to room temperature. The heating rate used throughout the experiment was 5 °C per minute. Experimental methods for the germanium oxides are included in the Supporting Information.

For electrochemical analysis, the samples were mixed with sodium carboxymethyl cellulose (Sigma Aldrich), polyacrylic acid (Sigma Aldrich), and Ketjenblack in a ratio of 80:5:5:10. De-ionized water was added to form a homogeneous slurry, which was then pasted on a copper foil using a doctor blade. 2016 type coin cells were assembled in an argon filled glove box using lithium metal as counter electrode, microporous polyethylene as separator, and 1.15 M $LiPF_6$ in ethylene carbonate/dimethyl carbonate/diethyl carbonate (EC/DMC/DEC; 3/4/3; Panax Starlyte) as electrolyte. The loading amount of active material for all electrodes was at least 1 $mg cm^{-2}$ and 1 g mL^{-1}. The specific capacities were calculated based on the active materials only (Ge/C).

Received: February 23, 2012
Revised: April 3, 2012
Published online: April 26, 2012

Keywords: electrochemistry · germanium · lithium-ion batteries · self-assembly

[1] a) M. G. Kim, S. Sim, J. Cho, *Adv. Mater.* **2010**, *22*, 5154 – 5158; b) J. Z. Chen, L. Yang, S. H. Fang, S. I. Hirano, *Electrochem. Commun.* **2011**, *13*, 848 – 851; c) Y. Q. Zou, Y. Wang, *ACS Nano* **2011**, *5*, 8108 – 8114.

[2] a) S. H. Ng, J. Z. Wang, D. Wexler, K. Konstantinov, Z. P. Guo, H. K. Liu, *Angew. Chem.* **2006**, *118*, 7050 – 7053; *Angew. Chem. Int. Ed.* **2006**, *45*, 6896 – 6899; b) C. K. Chan, H. L. Peng, G. Liu, K. McIlwrath, X. F. Zhang, R. A. Huggins, Y. Cui, *Nat. Nanotechnol.* **2008**, *3*, 31 – 35; c) H. Kim, J. Cho, *Nano Lett.* **2008**, *8*, 3688 – 3691; d) J. Cho, *J. Mater. Chem.* **2010**, *20*, 4009 – 4014; e) A. Magasinski, P. Dixon, B. Hertzberg, A. Kvit, J. Ayala, G. Yushin, *Nat. Mater.* **2010**, *9*, 353 – 358; f) N. S. Choi, Y. Yao, Y. Cui, J. Cho, *J. Mater. Chem.* **2011**, *21*, 9825 – 9840; g) K. Evanoff, A. Magasinski, J. B. Yang, G. Yushin, *Adv. Energy Mater.* **2011**, *1*, 495 – 498.

[3] a) H. Lee, M. G. Kim, C. H. Choi, Y. K. Sun, C. S. Yoon, J. Cho, *J. Phys. Chem. B* **2005**, *109*, 20719 – 20723; b) G. L. Cui, L. Gu, L. J. Zhi, N. Kaskhedikar, P. A. van Aken, K. Mullen, J. Maier, *Adv. Mater.* **2008**, *20*, 3079 – 3083.

[4] a) C. K. Chan, X. F. Zhang, Y. Cui, *Nano Lett.* **2008**, *8*, 307 – 309; b) Y. D. Ko, J. G. Kang, G. H. Lee, J. G. Park, K. S. Park, Y. H. Jin, D. W. Kim, *Nanoscale* **2011**, *3*, 3371 – 3375; c) M. H. Seo, M. Park, K. T. Lee, K. Kim, J. Kim, J. Cho, *Energy Environ. Sci.* **2011**, *4*, 425 – 428.

[5] M. H. Park, Y. Cho, K. Kim, J. Kim, M. L. Liu, J. Cho, *Angew. Chem.* **2011**, *123*, 9821 – 9824; *Angew. Chem. Int. Ed.* **2011**, *50*, 9647 – 9650.

[6] M. H. Park, K. Kim, J. Kim, J. Cho, *Adv. Mater.* **2010**, *22*, 415 – 418.

[7] L. C. Yang, Q. S. Gao, L. Li, Y. Tang, Y. P. Wu, *Electrochem. Commun.* **2010**, *12*, 418 – 421.

[8] M. G. Kim, J. Cho, *J. Electrochem. Soc.* **2009**, *156*, A277 – A282.

[9] a) G. L. Cui, L. Gu, N. Kaskhedikar, P. A. van Aken, J. Maier, *Electrochim. Acta* **2010**, *55*, 985 – 988; b) R. A. DiLeo, S. Frisco, M. J. Ganter, R. E. Rogers, R. P. Raffaelle, B. J. Landi, *J. Phys. Chem. C* **2011**, *115*, 22609 – 22614.

[10] X.-L. Wang, W.-Q. Han, H. Chen, J. Bai, T. A. Tyson, X.-Q. Yu, X.-J. Wang, X.-Q. Yang, *J. Am. Chem. Soc.* **2011**, *133*, 20692 – 20695.

[11] Z. Y. Yang, J. G. C. Veinot, *J. Mater. Chem.* **2011**, *21*, 16505 – 16509.

[12] J. Schwan, S. Ulrich, V. Batori, H. Ehrhardt, S. R. P. Silva, *J. Appl. Phys.* **1996**, *80*, 440 – 447.
[13] S. Yoon, C. M. Park, H. J. Sohn, *Electrochem. Solid-State Lett.* **2008**, *11*, A42 – A45.
[14] a) X. H. Liu, J. Y. Huang, *Energy Environ. Sci.* **2011**, *4*, 3844 – 3860; b) X. H. Liu, S. Huang, S. T. Picraux, J. Li, T. Zhu, J. Y. Huang, *Nano Lett.* **2011**, *11*, 3991 – 3997; c) X. H. Liu, H. Zheng, L. Zhong, S. Huan, K. Karki, L. Q. Zhang, Y. Liu, A. Kushima, W. T. Liang, J. W. Wang, J.-H. Cho, E. Epstein, S. A. Dayeh, S. T. Picraux, T. Zhu, J. Li, J. P. Sullivan, J. Cumings, C. Wang, S. X. Mao, Z. Z. Ye, S. Zhang, J. Y. Huang, *Nano Lett.* **2011**, *11*, 3312 – 3318.

